Statistical Properties of Precipitation Patterns

I. I. ZAWADZKI

Dept. of Meteorology, McGill University, Montreal, Canada

(Manuscript received 10 November 1972)

ABSTRACT

Space and time autocorrelation functions are defined for the precipitation process on a horizontal plane. An optical device was designed and used to measure these functions as well as the mean, the mean square, and the variance of the rainfall rate for a time sequence of precipitation patterns of a widespread convective storm. The input data were radar PPI records stored on film in which the transmittance was adjusted to be proportional to rainfall rate.

1. Introduction

In the last decade a number of statistical studies of precipitation patterns have been made. Kessler and Russo (1963) and Kessler (1966) prepared a computer program to determine a few points of the autocorrelation function of horizontal two-dimensional radar records or precipitation as well as other properties of the echo field. Cole (1964) devised a technique for analyzing echo patterns based on the assumption that the distribution of echo and non-echo points in a given direction is described by the random telegraph process. Wilson (1966) studied the movement and predictability of echo patterns of different scales by cross-correlating radar records of different times. Freeny and Gabbe (1969) analyzed rainfall rates from a dense network of fast response raingages. They obtained the frequency of occurrence of different rainfall rates and the conditional probabilities of rainfall rate, given the value at another point in space or a previous value at the same point. Austin and Houze (1970), using raingage records, obtained the variance spectra of rainfall rate looking for regularities between cells of precipitation.

Studies of this kind have direct practical applications. For example, Drufuca and Paraboni (1970) discussed the importance of precipitation statistics and, in particular, of the spatial autocorrelation function, in studying the effects of attenuation by rain on microwave links.

One difficulty with conventional correlation analysis of precipitation patterns is that the precipitation process is nonstationary and nonhomogeneous. The autocorrelation function (ACF) as defined in literature (Bendat and Piersol, 1966) thus contains two variables for every variable in the original function. The ACF of rainfall rate would therefore have four space and two time variables since the rainfall rate is function of position (x,y) and time (t).

In the present work the ACF is defined in a way which avoids this complication and at the same time is appropriate to the character of the phenomenon of precipitation.

To study the variability of rainfall rate as a function of space and time separately, a "space ACF" and "time ACF" will be defined. Since the storm system is in motion, the time variations, when observed from a fixed location on the ground, will be different from those observed from a position moving with the storm system. Accordingly, two different time autocorrelation functions will be defined depending on the observation point from which the time variations are considered.

The measurements of the time and space ACF's, as well as of the mean, mean square, and variance of the rainfall rate over an area, are obtained by an optical method which is described in Section 3.

2. Definitions and theory

Let $R(x,y,t)$ denote the rainfall rate as a function of space and time. Since storm systems are widely spaced each system can be considered an isolated phenomenon. Thus, an area S and time interval T can be determined such that

$$\left.\begin{aligned} &R(x,y,t)\gtrless 0, \quad \text{for } (x,y) \text{ inside } S \text{ and } t \text{ inside } T \\ &R(x,y,t)=0, \quad \text{outside this region} \end{aligned}\right\}. \tag{2.1}$$

The time-space autocorrelation function of R is defined over such an area S, large enough to contain the entire storm, and a time T longer than the storm's duration, by

$$A_{S,T}(\alpha,\beta,\tau)=\frac{1}{ST}\int_T\int_S R(x,y,t)R(x+\alpha, y+\beta, t+\tau) \times dxdydt, \tag{2.2}$$

where α, β and τ are the lag variables.

The subscripts emphasize the dependence on S and T. Since increasing S and T will not affect the value of the integral, $A_{S,T}$ falls off as $1/(ST)$. The normalized ACF, defined by

$$a'(\alpha,\beta,\tau)=\frac{A_{S,T}(\alpha,\beta,\tau)}{A_{S,T}(0,0,0)}, \tag{2.3}$$

will be independent of S and T so long as both are taken large enough to contain the entire storm system. Defined in this way, the normalized ACF has only as many variables as $R(x,y,t)$. It can be seen that the normalized ACF is an even function with a range between 0 and 1.

Notice that the definition of the ACF given here does not require the stationarity and homogeneity of $R(x,y,t)$. The properties of the conventional ACF, as defined for stationary and homogeneous processes, do not necessarily hold for the ACF defined here, particularly for large lags, and it is necessary to verify every property used.

To simplify notation, the average over T will be indicated by an overbar and the average over S by angle brackets. Eq. (2.2) thus becomes

$$A_{S,T}(\alpha,\beta,\tau)=\langle\overline{R(x,y,t)R(x+\alpha,\ y+\beta,\ t+\tau)}\rangle. \tag{2.4}$$

The instantaneous space ACF is defined by

$$A_S(\alpha,\beta)=\langle R(x,y,t)R(x+\alpha,\ y+\beta,\ t)\rangle. \tag{2.5}$$

The variable t on the left-hand side has been omitted for simplicity, although it is understood that $A_S(\alpha,\beta)$ corresponds to a time instant.

The time-averaged space ACF, denoted by $\overline{A_S(\alpha,\beta)}$, can be obtained by either averaging (2.5) over time or setting $\tau=0$ in (2.4), i.e.,

$$\overline{A_S(\alpha,\beta)}=A_{S,T}(\alpha,\beta,0)=\langle\overline{R(x,y,t)R(x+\alpha,\ y+\beta,\ t)}\rangle. \tag{2.6}$$

The Eulerian time ACF, denoted by $E_{S,T}(\tau)$, is obtained by setting $\alpha=\beta=0$ in (2.4). Thus,

$$E_{S,T}(\tau)=A_{S,T}(0,0,\tau)=\langle\overline{R(x,y,t)R(x,\ y,\ t+\tau)}\rangle. \tag{2.7}$$

The cross-correlation function of the rainfall rate pattern at two different times is defined by

$$\langle R(x,y,t_1)R(x+\alpha,\ y+\beta,\ t_2)\rangle. \tag{2.8}$$

There exist values of α and β, say α_0 and β_0, which will maximize this expression. These lags represent the linear displacement of the pattern $R(x,y,t_1)$ with respect to $R(x,y,t_2)$ which gives the best matching between the two. Therefore it is reasonable to define the vector displacement of the storm system during the interval (t_2-t_1) by the pair (α_0,β_0), as has been done by Wilson (1966). In general, α_0 and β_0 will depend on t_1 and $\tau=t_2-t_1$.

The velocity components of the storm system are defined by

$$U_x(t)=\lim_{\tau\to 0}\frac{\alpha_0}{\tau},\quad U_y(t)=\lim_{\tau\to 0}\frac{\beta_0}{\tau}. \tag{2.9}$$

For a constant velocity these expressions become

$$\alpha_0=U_x\tau,\quad \beta_0=U_y\tau. \tag{2.10}$$

A system of coordinates moving without rotation with the velocity of the storm system will be called storm coordinates (as opposed to fixed coordinates).

With reference to (2.4) it is now possible to define a Lagrangian time ACF [denoted by $L_{S,T}(\tau)$] by taking $\alpha=\alpha_0$ and $\beta=\beta_0$:

$$L_{S,T}(\tau)=A_{S,T}(\alpha_0,\beta_0,\tau)$$
$$=\langle\overline{R(x,y,t)R(x+\alpha_0,\ y+\beta_0,\ t+\tau)}\rangle. \tag{2.11}$$

While the Eulerian time ACF is dependent on the motion of the storm and changes in structure that occur within it, the Lagrangian time ACF is defined relative to the moving storm coordinates and therefore is independent of the storm's motion.

It should be noted that

$$A_{S,T}(0,0,0)=\overline{A_S(0,0)}=E_{S,T}(0)=L_{S,T}(0)=\langle\overline{R^2}\rangle, \tag{2.12}$$

where $\langle\overline{R^2}\rangle$ is the mean square value over S and T, of $R(x,y,t)$. The normalized ACF's are obtained (all of them independent of S and T) by dividing (2.6), (2.7) and (2.11) by $\langle\overline{R^2}\rangle$ and using (2.3) and (2.12):

$$\left.\begin{aligned}\overline{a(\alpha,\beta)}&=a'(\alpha,\beta,0)\\ e(\tau)&=a'(0,0,\tau)\\ l(\tau)&=a'(\alpha_0,\beta_0,\tau)\end{aligned}\right\}. \tag{2.13}$$

The instantaneous space ACF is normalized by dividing (2.5) by $A_S(0,0)=\langle R^2\rangle$ (the instantaneous mean square value) to obtain

$$a(\alpha,\beta)=\frac{A_S(\alpha,\beta)}{\langle R^2\rangle}. \tag{2.13a}$$

The terms $e(\tau)$, $l(\tau)$ and $a(\alpha,\beta)$ can be measured with the correlator described in the next section.

As an example, we now consider the special case in which the rainfall rate expressed in storm coordinates is independent of time. That is, if (x',y') are the storm coordinates and $R'(x'y',t)$ is the rainfall rate in these coordinates, then

$$R(x,y,t)=R'(x',y')=R'(x-U_xt,\ y-U_yt). \tag{2.14}$$

The Eulerian time ACF from (2.7) becomes in this case

$$E_{S,T}(\tau)=\overline{\langle R'(x-U_xt,\ y-U_yt)R'(x-U_xt-U_x\tau,\ y-U_yt-U_y\tau)\rangle}, \tag{2.15}$$

and the time averaged space ACF from (2.6) is

$$A_{S,T}(\alpha,\beta,0)=\overline{\langle R'(x-U_xt,\ y-U_yt)R'(x-U_xt+\alpha,\ y-U_yt+\beta)\rangle}. \tag{2.16}$$

If in (2.16) we take $\alpha=-U_x\tau$ and $\beta=-U_y\tau$, then by comparing (2.15) and (2.16) we have, in the direction of motion

$$E_{S,T}(\tau)=\overline{A_S(-U\tau)}=\overline{A_S(U\tau)},$$

where

$$U=(U_x^2+U_y^2)^{\frac{1}{2}}.$$

Using (2.12), we obtain

$$\overline{a(U\tau)}=e(\tau). \tag{2.17}$$

The validity of (2.17) for a storm system is an indication that the Taylor hypothesis (Taylor, 1938; Lumley and Panofsky, 1964) is applicable to the precipitation process. That is, the storm is statistically stationary in the sense that the properties of space variations can be obtained from time variations at a point by converting time into space through the velocity of the storm system. This does not require that the rainfall rate in storm coordinates be actually independent of time. That is, (2.14) is a sufficient but not a necessary condition that the Taylor hypothesis be satisfied.

Finally, and in general, the instantaneous variance of $R(x,y,t)$, $\sigma^2(t)$, is defined over the same region as the ACF:

$$\sigma^2(t)=\langle R^2\rangle-\langle R\rangle^2. \tag{2.18}$$

The variance of $R(x,y,t)$ taken over S and T is defined by

$$\begin{aligned}\overline{\sigma^2}&=\overline{\langle(R(x,y,t)-\langle R\rangle)^2\rangle},\\ &=\overline{\langle R^2\rangle}-\langle\bar{R}\rangle^2,\end{aligned} \tag{2.19}$$

which is different from the time average of (2.18). It is understood that $\langle R^2\rangle$ and $\langle R\rangle^2$ are time dependent. Both are also dependent on S. Since the storm is entirely contained within these intervals, the dependence of $\langle R^2\rangle$ is as $1/S$ while that of $\langle R\rangle^2$ is as $1/S^2$. In the same way $\overline{\langle R^2\rangle}\propto 1/ST$ and $\langle\bar{R}\rangle^2\propto(1/ST)^2$. Thus, the variance depends on S and T in a complicated fashion.

3. Instrumentation

a. Radar records

The precipitation patterns used in this work were obtained with the McGill FPS-18 weather radar, the parameters of which are given in Table 1.

In addition to the basic PPI display described by Marshall and Ballantyne (1970), a scope and a camera were used to obtain pictures with transmittance proportional to rainfall rate (see Appendix A). A half-tone filter over the cathode ray tube prevents any range effects due to trace overlapping (Gunn, 1963).

In this radar system the antenna undergoes a programed cycle in which azimuth and elevation are systematically varied to provide PPI pictures of many antenna elevations in each cycle. In this way any given elevation was swept every 4 min.

There are many reasons for choosing R instead of the reflectivity factor Z as the quantity to be analyzed. Rainfall rate is a quantity directly relevant in hydrology. It is nearly proportional to the specific attenuation of microwaves at many frequencies and therefore more convenient for attenuation studies. There is also the practical consideration that R, with a more limited dynamic range than Z, is easier to accommodate in the linear part of the response characteristic curve (gamma curve) of the display and the film.

b. The correlator

The first approach to the optical analysis of two-dimensional precipitation patterns was made by using a coherent light system to obtain power spectra. The method and results were described by Zawadzki and Rogers (1969). The main problem encountered with this method was the measurement of spectral content at small wavenumbers. The background light which formed most of the contribution in the center of the spectrum, where the wavenumber is zero, masked this region. Later it was found that this problem is avoidable and the method is worth further attention. However, as an alternative a system of data processing with incoherent light (described by Kovaszny and Arman, 1957) was chosen for its simplicity and economy. This straightforward method was further simplified in the present work.

The optical system is shown in Fig. 1. A pinhole located at the focal point of a lens selects all horizontal rays from a diffuse light source. Two photographic plates with transmittance proportional to rainfall rate are located between the light source and the lens. One plate is in a fixed position while the other can be

TABLE 1. Parameters of the McGill FPS-18 radar.

Wavelength	10.2 cm
Pulse length	0.3 km
Beam width	0.8°
Sensitivity at all ranges	$Z=160$ mm^6 m^{-3} ($R\approx 0.8$ mm hr^{-1})

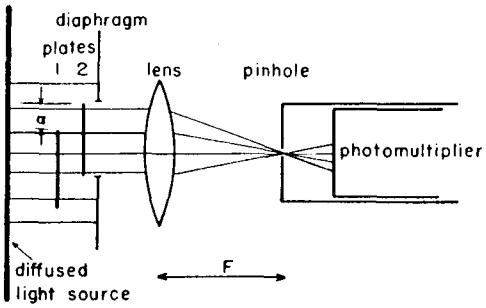

FIG. 1. Schematic diagram of the correlator.

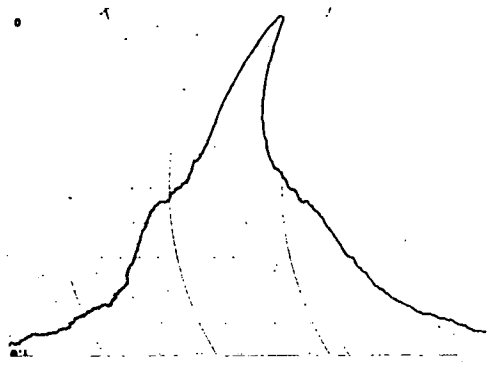

FIG. 2. An example of a section of an ACF as plotted by the chart recorder.

displaced in two perpendicular directions (x,y) normal to the direction of incident light.

If I is the intensity of a horizontal ray emerging from the light source, its intensity after passing through Plate 1 will be

$$IT_1(x,y),$$

where $T_1(x,y)$ is the transmittance function of Plate 1. Plate 2 is displaced with respect to Plate 1 by (α,β) and therefore the intensity reaching the lens is

$$IT_1(x,y)T_2(x+\alpha, y=\beta),$$

where $T_2(x,y)$ is the transmittance function of Plate 2.

The lens focuses all the rays into the pinhole, effectively performing the integration

$$I\int_{S_0} T_1(x,y)T_2(x+\alpha, y+\beta)dxdy,$$

where S_0 is the area of the diaphragm aperture. Since the transmittance function of the plates is proportional to the rainfall rate, the photomultiplier detects an amount of light proportional to

$$P(\alpha\beta)=\int_{S_0} R_1(x,y)R_2(x+\alpha, y+\beta)dxdy.$$

The movement of Plate 2 is controlled by two micrometer heads. The horizontal one is mechanically coupled to a chart recorder, such that the motor of the recorder drives Plate 2 across all values of α while β is constant. The deflection of the chart recorder measures $P(\alpha,\beta)$ from the amplified output of the photomultiplier (see Appendix B). The amplification is adjusted to obtain full-scale deflection for $P(0,0)$. In this way, for every value of β, a graph such as on Fig. 2 is obtained. This particular one corresponds to $P(\alpha,0)$. Ten to fifteen such graphs are used to plot half of a two-dimensional autocorrelation pattern. Only half of the pattern is needed since the ACF is an even function.

When two identical plates are inserted in the correlator the autocorrelation pattern as defined by (2.5)

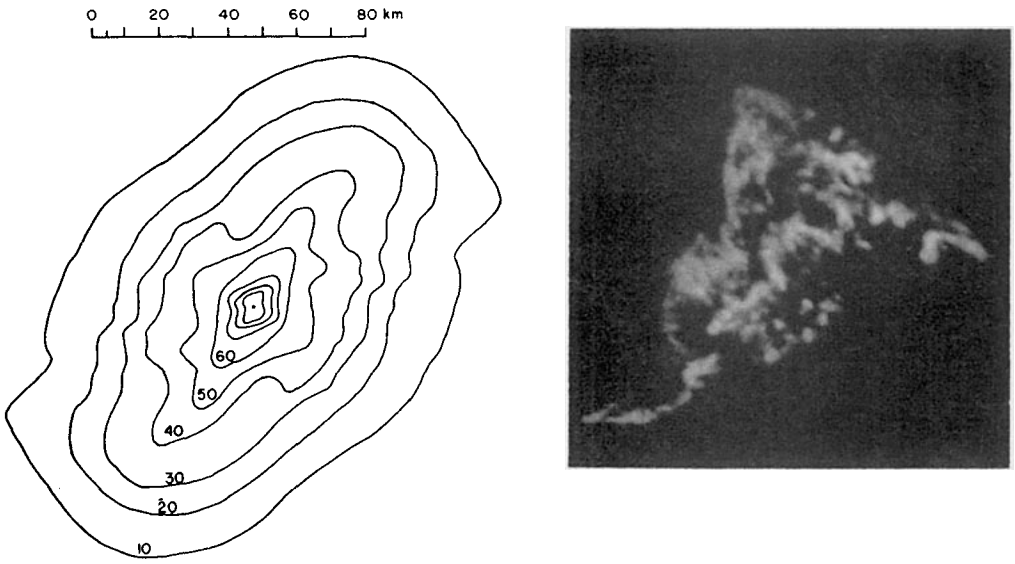

FIG. 3. The space normalized ACF as measured by the correlator (left) corresponding to the precipitation pattern of 12 September 1969 (right).

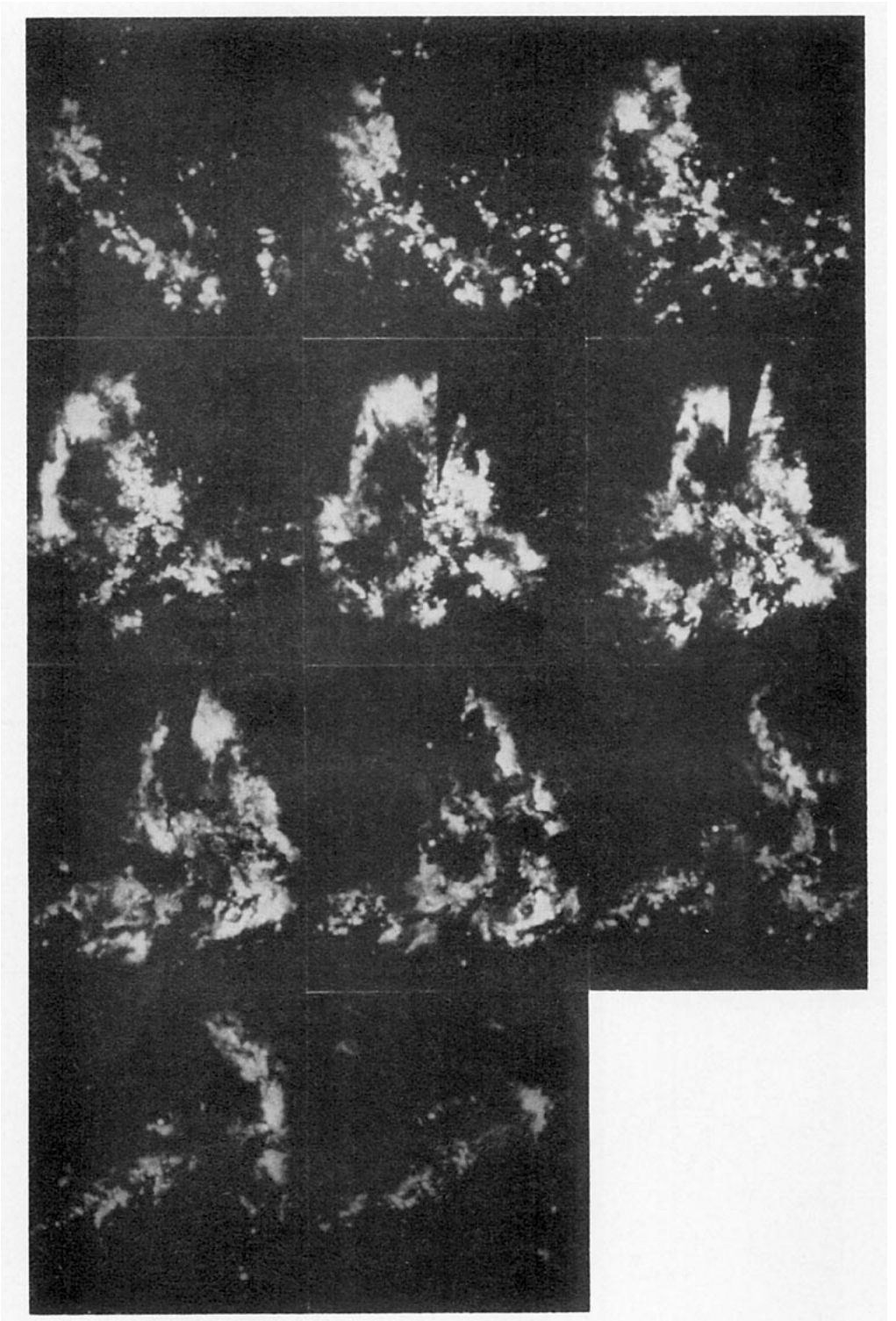

Fig. 4. A sequence of precipitation patterns at 16-min intervals of the storm of 16 September 1969 from 1102 to 1342 local time.

is obtained. In the same way, if the two plates contain different PPI pictures, the cross-correlation function is obtained.

An example of the ACF measured with the autocorrelator is shown in Fig. 3. The contours are isopleths of the ACF indicated as percentages of the maximum.

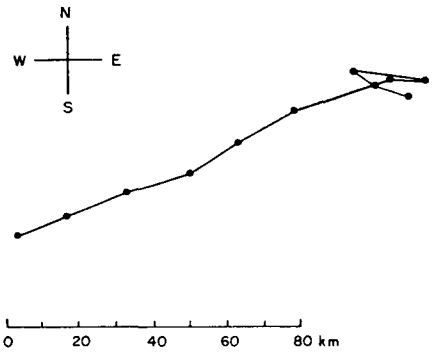

FIG. 5. Trajectory during the time period 1102–1342, as obtained by the cross-correlation method.

This autocorrelation pattern corresponds to the precipitation shown on the photograph which occurred on 12 September 1969.

To measure $\langle R^2 \rangle$ and $\langle R \rangle$ the system is calibrated using a filter of known uniform transmittance which covers a diaphragm located in the plate holder.

4. Measurements

Using the concepts developed in Section 2 and the instrumental techniques described in Section 3, the following quantities can be measured:

1. The instantaneous mean value $\langle R \rangle$ of rainfall rate over an area S
2. The instantaneous mean square value $\langle R^2 \rangle$ over the same area
3. The area of detectable precipitation
4. The velocity and trajectory of the storm system
5. The two-dimensional space autocorrelation function of the storm system
6. The Eulerian and Lagrangian time autocorrelation functions

All these measurements were taken for a sequence of radar PPI records from a storm system of 16 September 1969.

This storm of widespread convective precipitation underwent its entire life cycle within the range of the radar in approximately 8 hr. Eleven pictures, 16 min apart, covering the most intense period of the storm were analyzed. In Fig. 4 are shown the portions of the PPI's which contained precipitation. The maximum range of the PPI scope was 220 km. The first picture of the sequence corresponds to 1102 and the last to 1342 (local times), thus covering almost 3 hr. The first cell appeared at 0837 at 130 km and 210°. Thereafter, the system developed very slowly into the first picture of Fig. 4. It is in the analyzed period of 3 hr that most of the precipitation occurred. After a peak period the storm entered its dissipation stage and little significant precipitation remained after 1400. However, some weak cells were present until 1600.

The movement of a storm system is a combination of actual displacement of individual cells, propagation of the precipitation in already existing cells, and the effects of generation of new cells and dissipation of old ones. It is very difficult to separate these components. The overall effect is measured by the vector displacement (α_0,β_0) as discussed in Section 2. However, by comparing the storm motion with cell motion, the effect of generation and dissipation of cells can be separated from the other two.

By cross-correlating successive pictures the vector displacement of the storm system was measured for each 16-min time interval. The trajectory of the storm system, composed by the successive vector displacements, is shown in Fig. 5. Since only the displacement of the storm has been defined, the trajectory is not referred to any particular origin of coordinates.

For comparison some cell velocities were measured by following the geometrical center of each cell (Fig. 6). The results are summarized in Table 2.

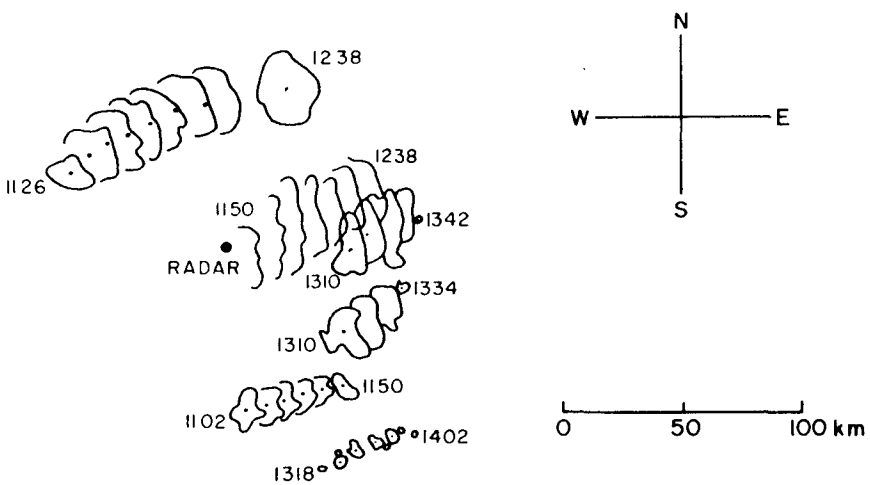

FIG. 6. Trajectories of some selected cells.

TABLE 2. Speeds of cells and the storm system (km hr^{-1}).

Time interval	Cell speed	Storm speed
1102–1134	63	60
1117–1150	65	65
1134–1254	79	73
1254–1342	64	7.5

A comparison of the two speeds shows that, during the development and peak periods of the storm, agreement between storm speed and cell speed is very good, although cells move slightly faster. During the dissipation period, however, the storm's speed is nearly zero while the cells continue to travel at only slightly slower speed. Following the cells during this stage shows that they dissipate at the front end of the storm. The direction of cell and storm movement is nearly the same, except at the dissipation stage. It thus appears that only at this stage is the dissipation of cells the dominant factor in determining the speed of the storm system.

In Fig. 7 are shown the variations with time of the square mean value of precipitation $\langle R\rangle^2$, the mean square value $\langle R^2\rangle$, and the variance σ^2, over a fixed area of 3.14×10^4 km^2. Although the storm lasted for nearly 8 hr, and extended over a considerable area for $3\frac{1}{2}$ hr, most of the activity happened in a period of $1\frac{1}{2}$ hr. The peak values of $\langle R\rangle^2$ and $\langle R^2\rangle$ are 5 (mm hr^{-1})^2 and 23 (mm hr^{-1})^2, respectively, and were reached simultaneously at approximately 1200. A visual inspection of the PPI's from times outside the 1100–1400 period indicated that the mean value of R increased very slowly and uniformly from zero to the value at 1100, and decreased after 1400 in the same way. In terms of total amount of precipitation the contribution from these periods was negligible.

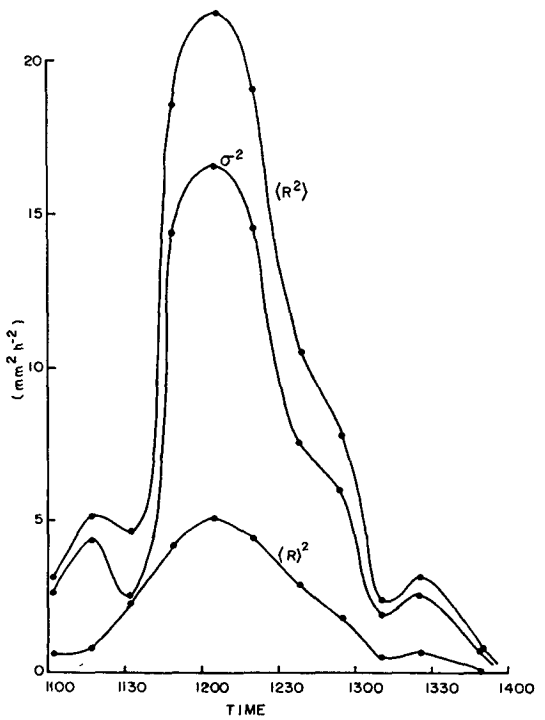

FIG. 7. Variation with time of $\langle R^2\rangle$, $\langle R\rangle^2$ and σ^2 of the precipitation below cloud base.

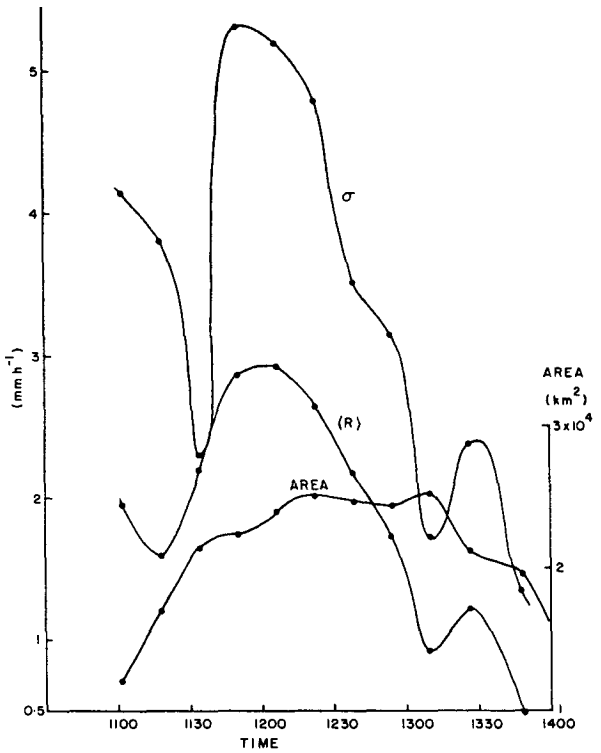

FIG. 8. Variation with time of $\langle R\rangle$, σ (both taken over the actual area of precipitation), and of area of precipitation.

More revealing is Fig. 8, where the values of $\langle R\rangle$ and σ were taken over the actual area of precipitation. The variation of the area of precipitation is also shown. This diagram shows that at first there are isolated small cells of precipitation with appreciable variability as indicated by small area, relatively low $\langle R\rangle$, and high σ. As the area grows the precipitation becomes more uniform while increasing in mean value. Then suddenly the variability increases while the area changes very little. In the decaying stage, σ and $\langle R\rangle$ decrease together while the area still remains nearly the same. Finally, after a second peak in $\langle R\rangle$ and σ, the three quantities decrease together with the intense parts dissipating faster.

If values of $\langle R\rangle^2$, $\langle R^2\rangle$ and σ^2 from Fig. 7 are plotted against each other as in Fig. 9, a rough proportionality between these quantities is found. Analytically,

$$\left.\begin{aligned}\langle R^2\rangle &= 4.35\langle R\rangle^2\\ \langle R^2\rangle &= 1.3\sigma^2\end{aligned}\right\}. \tag{4.1}$$

To obtain the time correlation functions as defined in (2.13), a set of measurements of the cross-correlation

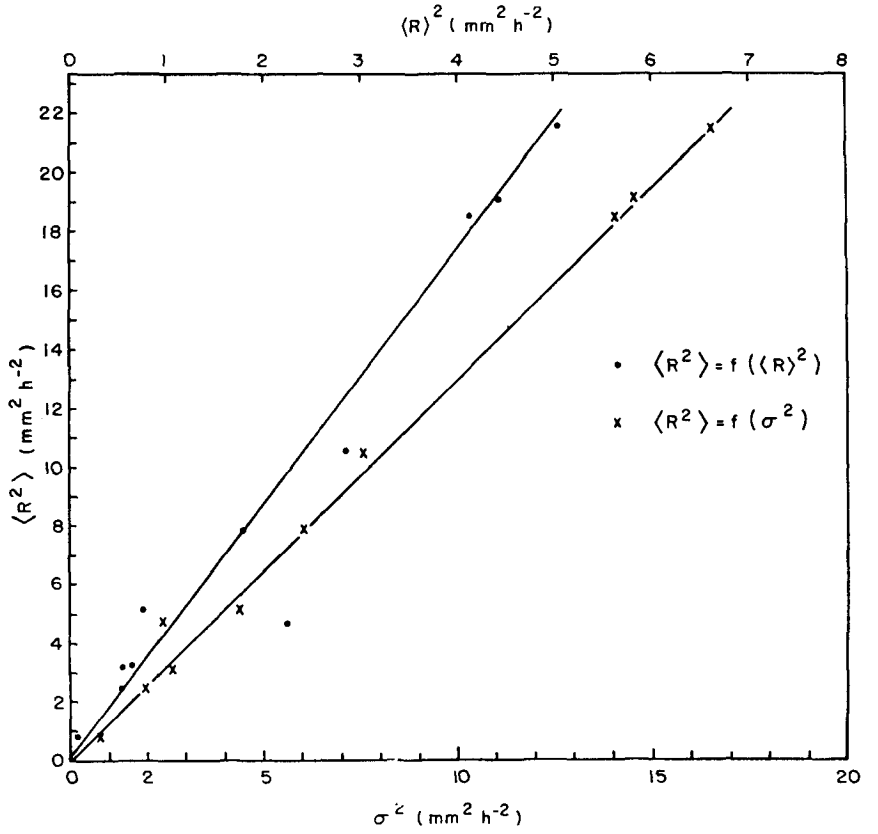

FIG. 9. Values of $\langle R^2 \rangle$ as functions of $\langle R \rangle^2$ and σ^2.

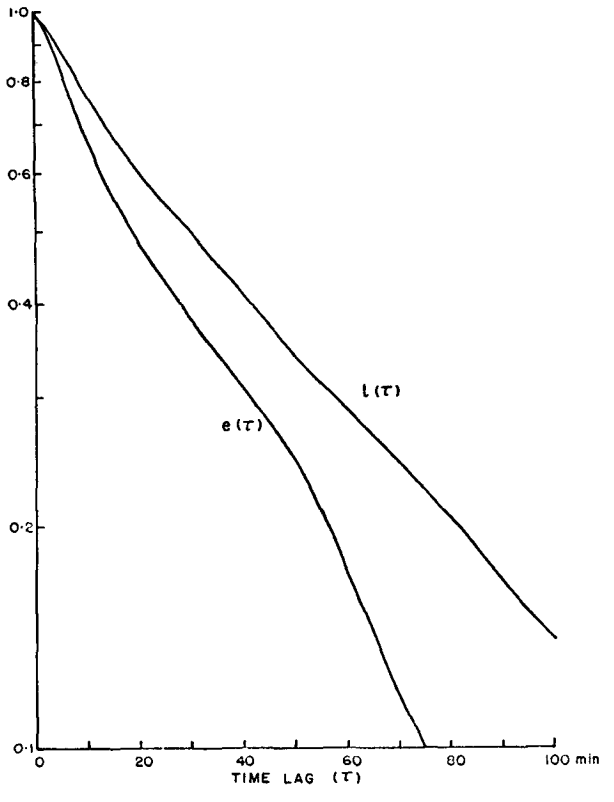

FIG. 10. Eulerian and Lagrangian normalized time ACF's.

function

$$\langle R(x,y,t)R(x+\alpha, y+\beta, t+\tau)\rangle \qquad (4.1a)$$

is made for every t and τ. For the Eulerian time ACF, the two plates are always held in fixed positions (that is, $\alpha=\beta=0$), while for the Lagrangian time ACF, α and β are chosen to maximize the expression (4.1a) in every measurement. In this way two sets of 11×11 values of (4.1a) were obtained. These values were averaged over time for every time-lag τ and then divided by the value for $\tau=0$ to obtain the normalized time ACF. The results are shown in Fig. 10. Since pictures were analyzed only every 16 min, the measured points are spaced by 16 min and smooth interpolation was made in between. In fact, pictures of the entire life cycle could have been used for this purpose, but the contribution from the times outside the analyzed period is very small and would not alter the curves of Fig. 10. Both time ACF's have a near-exponential form. The decorrelation time, defined as the value of τ for which the time ACF falls to $1/e$ of its maximum value, is 32 min and 44 min for the Eulerian and Lagrangian time ACF's, respectively.

Fig. 11 shows the set of patterns of normalized space ACF's. The curves are lines of constant decorrelation, and the numbers indicate percentage of maximum. The large-scale features correspond to the visual impression given by the storm patterns of Fig. 4. The

FIG. 11. Normalized space ACF's at 16-min intervals covering the period 1102–1342 of the storm of 16 September 1969.

major axis of the ACF's at large lags is nearly perpendicular to the direction of motion during the growth period, and gradually becomes nearly parallel to it in the dissipation stage. When ellipticity of the pattern for small lags is evident, the major axis tends to be perpendicular to that for large lags (particularly at 1206). Usually, however, the large-scale pattern shows strong ellipticity, while for small lags the pattern is

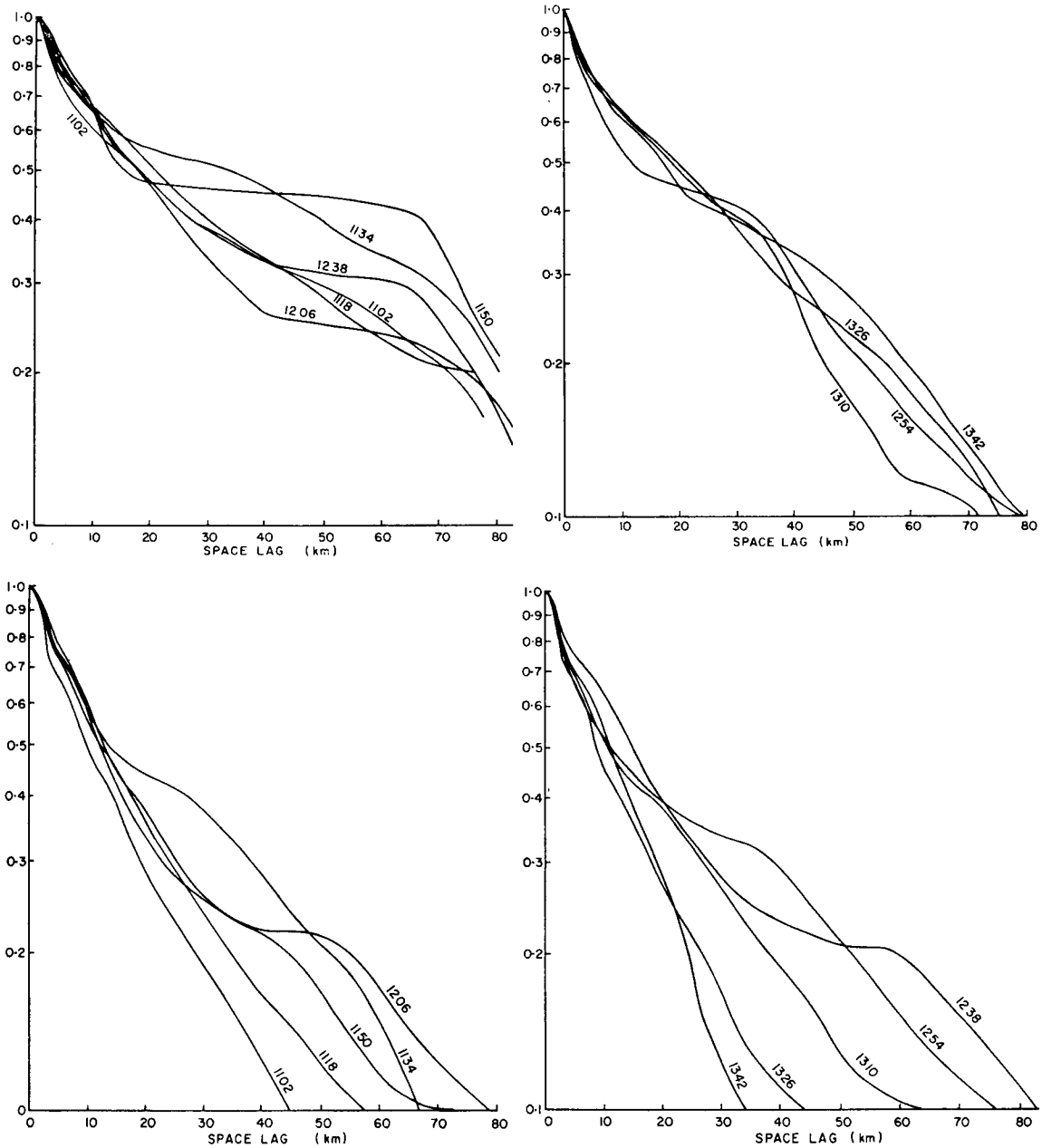

FIG. 12. Sections of the normalized space ACF's along the major (upper panels) and minor (lower panels) axes of the 40% curves of Fig. 11.

nearly circular. This indicates that within small scales the precipitation field is nearly isotropic.

Secondary maxima appear clearly in some cases, showing periodicities of 50–70 km. The most striking case is at 1206 where strong secondary maxima at the 40% level occur. It is easy to identify the origin of them in Fig. 4 as the three clusters of cells oriented along the NW–SE line. However, the 10% level maxima are not so obvious.

Two sets of sections made along the major and minor axis of the 40% curve are shown in Fig. 12. Except for the secondary maxima, all the curves show near exponential behavior. There is a suggestion that for small lags the curves are steeper than for large lags.

The decorrelation distance in a particular direction will be defined here as the value of the space lag for which the space ACF in this particular direction has a value of $1/e$ of its maximum. There is no special reason for defining the decorrelation distance this way. Any value of the ACF would be as good for this purpose. However, the nearly exponential behavior of the ACF's makes this choice a rather natural one.

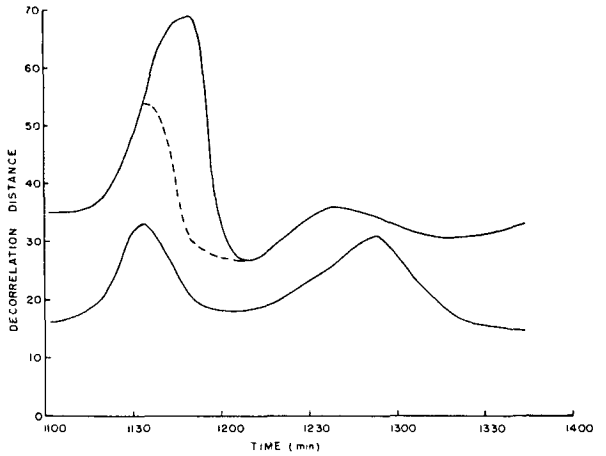

FIG. 13. Decorrelation distances to $1/e$ along the major (upper curve) and minor (lower curve) axes of the 40% curves of Fig. 11. The dashed line results when the effects of the secondary maxima are eliminated by extrapolation in the ACF patterns.

This decorrelation distance for the curves in Fig. 12 is shown as function of time in Fig. 13. The dashed line is obtained when the effects of the secondary maxima are eliminated by extrapolation in the ACF patterns. As seen, the decorrelation distance is nearly constant in spite of the changes in the patterns. For the minor axis it is around 20 km and for the major axis about 35 km.

Fig. 14 represents the normalized average space ACF, $\overline{a(\alpha,\beta)}$. The anisotropy for small scales has disappeared completely in the average. The large-scale features are similar to the individual autocorrelation patterns. The decorrelation distances as defined previously are 24 and 37 km, respectively, in the directions of the minor and the major axis of the 40% curve.

In Fig. 15 the two normalized time ACF's are again presented together with the time-averaged space ACF, defined by

$$\overline{a(U\tau)}=\frac{1}{T\langle R^2\rangle}\int_0^T A_S[U(t)\tau,t]dt,$$

with the scale of space lag in the direction of motion converted to $U(t)$.

It is seen that $\overline{a(U\tau)}$ falls just below $e(\tau)$ for time lags shorter than 37 min, and between $e(\tau)$ and $l(\tau)$ for larger τ. The behavior for small lags runs contrary to intuition since it would be reasonable to expect $e(\tau)$ to be the lowest curve as it combines both space and time variability. The observed behavior could arise from a complicated relationship between the time and space dependence, resulting from a constant generation of precipitation at the rear of the cells. However, the position of $\overline{a(U\tau)}$ is very sensitive to the velocity of the storm, and since the difference between $e(\tau)$ and $\overline{a(U\tau)}$ is small it could be due to experimental errors. In any case the proximity of the two curves for $\tau<40$ min

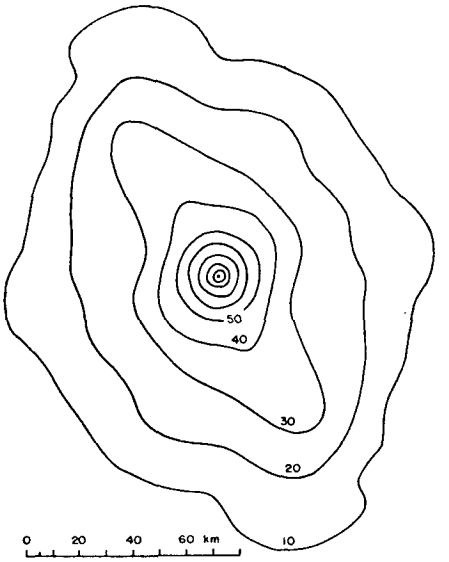

FIG. 14. Time-averaged space ACF.

indicates the validity of the Taylor hypothesis. In particular, for periods $\leqslant 40$ min, the statistical properties of precipitation as functions of space (in the

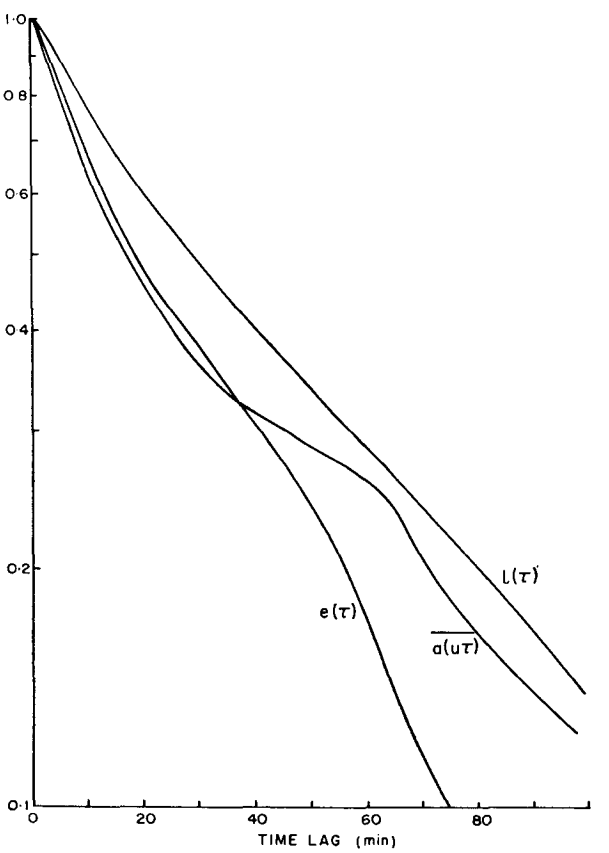

FIG. 15. The time-averaged space ACF, with the scale of space lag converted to time scale, together with the Eulerian and Lagrangian time ACF's.

direction of storm motion) can be obtained from time records of a network of raingages. For periods >40 min this is not valid. It should be noticed that this result was obtained with data smoothed in space, by the radar beam, and the display, and is not necessarily valid if data with less smoothing are processed.

5. Summary

The ACF of the rainfall rate is defined as a function of time and space on a horizontal plane [Eq. (2.2)]. By defining this ACF over a time period longer than the storm's duration and over an area large enough to contain the entire storm during its life cycle, the normalized time-space ACF becomes independent of this area and time period, and is a function only of the two space lags and the time lag. The variance, mean, and mean square rainfall rate are defined over the same region and time and depend on the area and time period. By taking the time lag equal to zero the space ACF is obtained [Eq. (2.6)]. Similarly, by taking the space lags equal to zero the Eulerian time ACF results [Eq. (2.7)]. When the space lags are taken to be equal to the components of the vector displacement of the storm, the Lagrangian time ACF is obtained [Eq. (2.11)].

The three ACF's, the mean, and the mean square rainfall rate, as well as the vector displacement of the storm, were measured with the correlator described in Section 3. The data used for this purpose were obtained with radar and stored on film in which the transmittance was made proportional to rainfall rate. The autocorrelator performed satisfactorily, providing an inexpensive and fast method of data processing for these specific measurements. The delicate part of the method is in the careful processing required to obtain the desired proportionality between transmittance and rainfall rate.

A complete set of measurements was made for the storm of 16 September 1969. Eleven pictures, 16 min apart and covering the most intense period of the storm, were used for analysis (Fig. 4). The results, described in Section 4, show that:

1) The velocity of this storm is nearly the same as that of individual cells during the period of intense precipitation. At the dissipation stage, however, the cells continue their motion until they reach the front of the storm where the dissipation process takes place, while the storm itself remains nearly motionless.

2) The storm shows a sudden increase in activity after nearly 3 hr of slow development. It reaches a peak after a half-hour of rapid buildup with a mean rainfall rate of 2.2 mm hr^{-1} over an area of 3.14×10^4 km^2. After this peak, the dissipation stage begins with an hour of fast decrease of the mean rainfall rate followed by three hours of slow dissipation.

3) The square mean and the mean square rainfall rate are roughly proportional.

4) The rainfall rate decorrelates nearly exponentially with time, the decorrelation time to $1/e$ being 32 min for the Eulerian and 44 min for the Lagrangian normalized time ACF's.

5) Within scales of the order of 10 km the precipitation is nearly isotropic. For larger scales, the space ACF's show an elliptic pattern. Sections of the normalized space ACF in a particular direction are nearly exponential with decorrelation distances to $1/e$ between 20 and 35 km.

6) The Taylor hypothesis holds for time periods shorter than 40 min.

Acknowledgments. The author is greatly indebted to Dr. R. R. Rogers, whose many comments and suggestions at every stage of this work are very much appreciated. Financial support to the author was provided by a grant from the Atmospheric Environment Service of Canada and a contract from the Canadian Department of Communications. The radar was provided to McGill University by the U. S. Air Force Cambridge Research Laboratories.

APPENDIX A

Calibration of the Photographic Plates

To obtain the desired relationship between the transmittance of the pictures and rainfall rate, the response of every stage of the system has to be considered. The voltage applied to the cathode ray tube (CRT) is

$$V=c\log Z.$$

The CRT has a power law response over a limited dynamic range. Thus, the luminance L in this range is given by

$$\log L=\gamma_T V=\gamma_T c\log Z,$$

where γ_T is the exponent in the power law.

When photographed, the density on negative film is

$$D_N=\gamma_N\log L+a_1,$$

where γ_N is the gamma of the negative and a_1 is a constant governing the total exposure.

Two identical positive contact copies are made for every frame to be analyzed. The density of the positives is

$$D_P=a_2-\gamma_P D_N,$$

with the constants having the same meaning as for the negatives. Therefore,

$$D_P=a_3-\gamma_P\gamma_N\gamma_T c\log Z.$$

The transmittance of the positives is

$$T=\exp(-I_P)=\exp(\log Z^b-c_3),$$

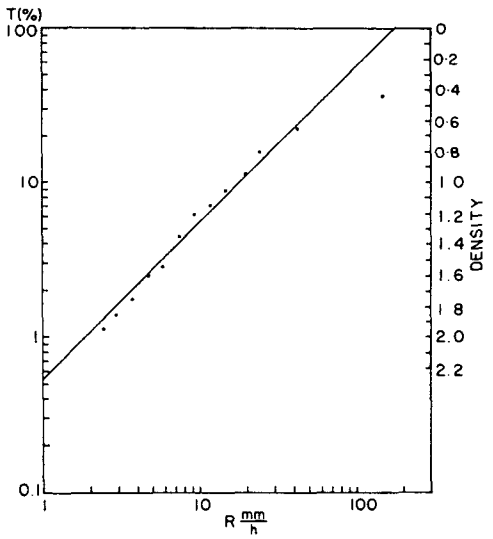

FIG. A1. Calibration curve for the plates of the storm of 16 September 1969.

where $b=\gamma_P\gamma_N\gamma_T c$. Thus, we may write

$$T=aZ^b.$$

Careful photographic processing of the positives enables control of γ_P to compensate for any variation in the other constants and thus maintain b equal to the exponent in the $Z-R$ relationship. The value of b used corresponds to the Marshall and Palmer equation. Periodical gray-scale test patterns on the film help to maintain the transmittance proportional to rainfall rate. A more thorough discussion on quantitative radar display is given by Legg (1960).

In Fig. A1 the actual relationship between transmittance of positives and rainfall rate is shown for September 69.

APPENDIX B

The Correlator

The correlator is built around an old slide projector Delineascope D with a light source of 500 W. A heat absorbing glass is attached to protect the plates. Next to it is mounted a diffusing glass, followed by the plate holder. The holder is built such that one of the plates could be displaced in two perpendicular directions, the displacement being controlled by micrometer heads. The horizontal movement is coupled mechanically to the motor drive of an Esterline-Angus Graphic Ammeter Model AW. The light passing through the two plates is focussed on a pinhole by a Kodak TV lens with a focal length of 150 mm. The photosensitive element is an RCA 7767 photomultiplier, located at a distance from the pinhole such that all the light falls on a small area of the cathode to minimize the effects of non-uniformity in the sensitivity of the cathode. The photomultiplier was shielded with a μ-metal tube. The signal is amplified by a two-stage amplifier and used to deflect the ammeter. The amplifier has controls which permit the full dynamic range of the signal to be accommodated in the full range of the ammeter.

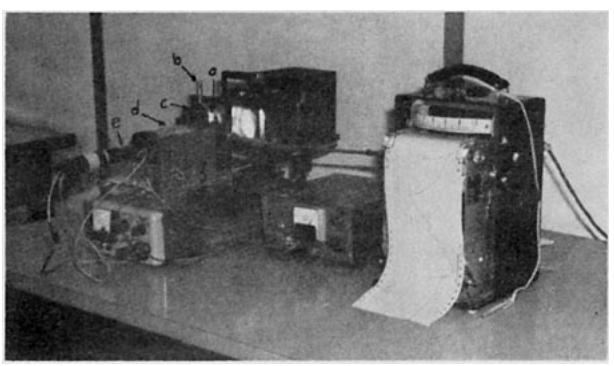

FIG. B1. The correlator: a, diffusing glass; b, vertical micrometer head; c, plate holder; d, lens; e, photo-multiplier; f, amplifier.

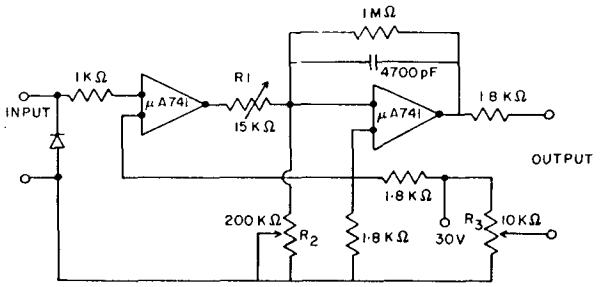

FIG. B2. Circuit diagram of the amplifier.

A photograph of the correlator is shown on Fig. B1, and the amplifier circuit diagram in Fig. B2.

REFERENCES

Austin, P. M., and R. A. Houze, Jr., 1970: Analysis of mesoscale precipitation areas. *Preprints 14th Radar Meteorology Conf.*, Tucson, Ariz., Amer. Meteor. Soc., 329–334.

Bendat, J. S., and A. G. Piersol, 1966: *Measurements and Analysis of Random Data.* New York, Wiley, Chap. 9.

Cole, J. W., 1964: Statistics related to shape and scale of pattern elements. Final Rept., Contract Cwb-10709, Travelers Research Center, Hartford, Conn.

Drufuca, G., and A. Paraboni, 1970: Some theoretical considerations on the rain attenuation parameters affecting millimetric radiolink design. *Alta Freq.*, **39**, 387-115E–391–119E.

Freeny, A. E., and J. D. Gabbe, 1969: A statistical description of intense rainfall. *Bell System Tech. J.*, July–August, 1789–1851.

Gunn, K. L. S., 1963: Tube-face filters for line spacing compensation. *Preprints Tenth Weather Radar Conf.*, Washington, D. C., Amer. Meteor. Soc., p. 361.

Kessler, E., 1966: Computer program for calculating average length of weather radar echoes and pattern bandedness. *J. Atmos. Sci.*, **23**, 569–574.

——, and J. A. Russo, 1963: Statistical properties of weather radar echoes. Preprints *Tenth Weather Radar Conf.*, Washington, D. C., Amer. Meteor. Soc., 25–33.

Kovaszny, L. S. G., and A. Arman, 1957: Optical autocorrelation measurement of two-dimensional random patterns. *Rev. Sci. Instr.*, **29**, 793–797.

Legg, T. H., 1960: The quantitative display of radar weather patterns on a scale of gray. Sci. Rept. MW-31, Stormy Weather Group, McGill University, Montreal.

Lumley, J. L., and H. A. Panofsky, 1964. *The Structure of Atmospheric Turbulence.* New York, Wiley.

Marshall, J. S., and E. Ballantyne, 1970: McGill weather radar: New research and remote displays. *Preprints 14th Radar Meteorology Conf.*, Tucson, Ariz., Amer. Meteor. Soc., 407–410.

Taylor, G. I., 1938: The spectrum of turbulence. *Proc. Roy. Soc. London*, **A164**, 476–490.

Wilson, J. W., 1966: Movement and predictability of radar echoes. Final Rept. 7471-204, The Travelers Research Center, Inc., Hartford, Conn.

Zawadzki, I. I., and R. R. Rogers, 1969. Two-dimensional spectra of precipitation patterns by coherent optical analysis. Tech. Rept. MWT-5, Stormy Weather Group, McGill University, Montreal.